

Jets and the shaping of the giant bipolar envelope of the planetary nebula KJpN 8

W. Steffen

Department of Physics and Astronomy, University of Manchester, Oxford Rd., Manchester, M13 9PL, UK

J. A. López,

Instituto de Astronomía, UNAM, Apdo. Postal 877, Ensenada, B.C. 22800, México.

ABSTRACT

A hydrodynamic model involving cooling gas in the stagnation region of a collimated outflow is proposed for the formation of the giant parsec-scale bipolar envelope that surrounds the planetary nebula KJpN 8. Analytical calculations and numerical simulations are presented to evaluate the model. The envelope is considered to consist mainly of environmental gas swept-up by shocks driven by an episodic, collimated, bipolar outflow. In this model, which we call the “free stagnation knot” mechanism, the swept-up ambient gas located in the stagnation region of the bow-shock cools to produce a high density knot. This knot moves along with the bow-shock. When the central outflow ceases, pressurization of the interior of the envelope stops and its expansion slows down. The stagnation knot, however, has sufficient momentum to propagate freely further along the axis, producing a distinct nose at the end of the lobe. The model is found to successfully reproduce the peculiar shape and global kinematics of the giant bipolar envelope of KJpN 8.

Subject headings: hydrodynamics: numerical — Planetary nebulae: individual KJpN 8— kinematics and dynamics—jets and outflows

1. Introduction

The planetary nebula KJpN 8 is surrounded by an expanding giant ($14' \times 4'$) bipolar envelope which so far is unique in its kind (López et al. 1995). The physical dimensions of the envelope as measured along the main axis and along the latest secondary outflows have been estimated to be 4.1×1.2 pc, respectively, for a distance of 1 kpc, corresponding to

0.3 pc arcmin⁻¹ (López et al. 1995). This size has to be compared with the diameter of the compact core which is only $\approx 4''$ across. Typical PNe have sizes of only a fraction of a parsec.

The main bipolar structure presents a tubular shape in the central region that decreases in radius in a peculiar way at increasing distance from the central source. The expansion speed of this ‘tube’ perpendicular to its main axis is $\approx 40 \text{ km s}^{-1}$ over a large angular extent and $\approx 160 \text{ km s}^{-1}$ along it (López et al. 1997). In addition to its huge dimensions and peculiar morphology, the bipolar envelope of KJPN 8 presents intriguing ripples across its structure, some of which mark the locations of strongly decreasing radius, culminating in the NE lobe in a narrow nose with a bright knot at the tip. The end of the SW lobe is less well defined but follows a similar pattern.

The morphology of KJPN 8 has been interpreted as the result of the action of a bipolar, rotating episodic jet or BRET (López et al. 1995). There is strong morphological and kinematical evidence that the ejection direction of the main bipolar outflow has changed with time. There is at least one additional kinematic subsystem to the main envelope which seems to be related to more recent ejections at a projected orientation of $\sim 50^\circ$ with respect to the axis of the main envelope. Observed radial velocities of symmetric emission line knots in these regions are as high as $\pm 220 \text{ km s}^{-1}$. The structure of these secondary bipolar jets suggests a large opening angle of the outflow, of up to 70° (López et al. 1995; López et al. 1997). Meaburn (1997) has recently derived proper motions of individual knots at the heads of these secondary outflows which combined with a simple bow-shock model yield a distance of $1600 \pm 230 \text{ pc}$ for KJPN 8. With this new distance the angular dimensions transform into $6.5 \times 1.8 \text{ pc}$.

Vázquez, Kingsburgh & López (1998) have obtained low resolution spectra of the core of KJPN 8 finding it to be a low excitation type I PN. The nebula seems to have been formed from a massive progenitor within a metal-rich environment, in agreement with its location right in the galactic plane. In addition, spectra of some knots and faint regions obtained in the nebular envelope indicate very low electron densities, ranging from 100 to 300 cm^{-3} . Recently, Huggins et al. (1997) and Forveille et al. (1998) have detected the presence of a remarkable expanding molecular CO torus in the core of KJPN 8 whose plane is perpendicular to the secondary, high-velocity bipolar outflows.

In this paper we explore a mechanism which we call the “free stagnation knot” to explain the peculiar characteristics of the giant bipolar envelope of KJPN 8. In this model the shocked ambient gas in the stagnation region of the bow-shock of a supersonic jet has sufficient time to cool in the vicinity of the symmetry axis to form a dense massive knot, moving at the advance speed of the bow-shock. After the outflow shuts off, the pressure in the nebula falls and the expansion speed of the existing envelope drops. The newly formed dense knot,

however, has sufficient momentum to continue its motion opening a narrow channel along the axis. Analytical calculations and time-dependent hydrodynamical simulations are presented and confronted with the existing observations.

2. The collimated outflow

An $H\alpha$ mosaic of KJPN8 (López et al. 1995) is presented in the top panel of Figure 1, a blow-up of the north east extreme of the nebula is shown in the bottom panel of this figure.

The extended envelope of KJPN 8 requires that the density of the jet be much smaller than that of the ambient medium, a behaviour similar to that found in extragalactic jets (Norman, Smarr and Winkler, 1985). The velocities involved here are, however, only of the order of a thousand kilometers per second as compared to velocities close to the speed of light in extragalactic jets. Radiative cooling will therefore be important, mainly for the shocked ambient medium. Some aspects of jets with cooling in internal shocks have been simulated numerically by e.g. Blondin, Fryxell and Königl (1990). The creation of elongated envelopes from stellar winds propagating into an inhomogeneous ambient medium has been investigated semi-analytically by Icke (1988) for the case of the radio nebula W50 around the X-ray binary SS433. The dynamics of radiative bow-shocks of continuous adiabatic jets has been investigated by Steffen et al. (1997, and references therein). These investigations show that an adiabatic jet results in an overall elongated ellipsoidal or cylindrical shape of the envelope. Due to quasi-periodic vortex-shedding in the bow-shock region, it is common to find large-scale ripples in the envelope superimposed on smaller scale ones which are caused by instabilities. However, the overall shape always has a convex curvature. From the existing studies it is clear that the cone-like structure of the envelope in KJPN 8 cannot be produced with a continuous low-density jet without cooling of the jet itself or a drastic structural anomaly in the bow-shock region.

In order to obtain a baseline for the parameter space for our numerical model of the envelope of KJPN 8 some basic properties of the outflow are estimated assuming a continuous non-radiative jet. The optically emitting envelope of swept-up ISM gas around the cocoon of a supersonic jet propagating into a uniform medium is now considered.

The expansion speed transverse to the axis of the main envelope is $v_t \approx 40 \text{ km s}^{-1}$. The envelope is somewhat asymmetric near the base (see Figure 1). Assuming axial symmetry, a radius $r_0 \approx 0.4 \text{ pc}$ and a length of $l \approx 2 \text{ pc}$ for the distance from NE tip to the core is adopted. The radius for the minor axis of the envelope of 0.4 pc is found by considering the distance from the core to the filament that traces the envelope located directly south of

the core, thus avoiding the deformation produced by the high-velocity jets on the envelope, where the radius would amount to 0.6 pc (López et al. 1995). Considering that the transverse expansion speed has been constant over the life-time of the nebula, its age can be estimated to be $t \sim 10^4$ yr. It is, however, likely to be smaller by a factor of two or so, since the expansion speed must have been higher in the initial stages of the expansion.

Using as age $t = 10^4$ yr and a propagation distance $l = 2$ pc we find that the mean advance speed of the bow-shock of the jet is ~ 200 km s⁻¹. Here we have also assumed that the ejection along the main axis has stopped only recently on this time-scale (i.e. we ignored the apparent recent changes in direction of the ejection). This bow-shock speed is low enough to be in the radiative shock regime, which is consistent with the observation that the NE lobe of the nebula can be observed up to the tip of the bow-shock. The SW lobe, however, does not show a bright tip at its end, possibly indicating that the shocked ISM collected by the bow-shock has not fully cooled yet. This could imply either that the ratio between the density of the jet and ambient medium has been higher here or that the jet itself had a higher speed than in the NE half of the nebula. If the age is smaller than 10^4 yr, as suggested above, the average advance speed would of course be higher too. As a working value for the advance speed of the outflow we shall therefore adopt $v_{\text{jh}} \approx 400$ km s⁻¹.

The observations suggest that there is variability in the direction of the outflow. Furthermore, the zonal structure of the nebula along the symmetry axis suggests a possible intermittence of the ejection. Note, however, that a similar structure can be produced by vortex-shedding in the bow-shock region or instabilities in the thin shell (e.g. Steffen et al. 1997).

The detection of the thin envelope near the end of the nebula requires that the mean advance speed of the jet be of the order of a few hundred kilometres per second. It also follows that the true advance speed of the active outflow has to be relatively moderate, about 1000 km s⁻¹, otherwise the cooling time would be too large to make it observable in H α within the lifetime of the nebula. For instance, at an ambient density of 100 cm⁻³ and a bow-shock velocity of 1000 km s⁻¹ the cooling time in the stagnation region would be around 40000 yr and for lower densities proportionally higher. Thus, the advance speed has to be considerably less than 1000 km s⁻¹. If the mean advance speed is of the order of 200 km s⁻¹ the outflow cannot have been switched off for a time significantly longer than the time it was on during the duty cycle. Otherwise the true advance speed would have to be too large to provide the observed mean speed with a cooling time short enough for the formation of the cool envelope. The cooling time increases with a high power (>3) of the shock velocity, whereas the mean advance speed is roughly proportional to the ratio between the time that the jet is switched on and the full duty-cycle. For the overall dynamics and

energetics the possible intermittence will have no large effect on our estimates, therefore we assume a continuous outflow for the global estimates of the nebula. Simulations show, however, that intermittence can have some influence on the overall shape of the envelope. From the segmented structure of the envelope on a scale of roughly 0.5 pc for each segment and an estimated bow-shock advance speed of $\approx 400 \text{ km s}^{-1}$, the duty cycle is around 4×10^{10} seconds.

For our estimates of the physical properties of the envelope and the jet we assume a conical shape of the nebula and use the dimensions of the NE lobe. First we estimate the density of the undisturbed medium into which the nebula expands. We use the measured expansion velocity of $v_r = 40 \text{ km s}^{-1}$, typical mass-loss rates \dot{M}_j between 10^{-8} and $10^{-6} M_\odot \text{ yr}^{-1}$ (Hutsemékers & Surdej 1989) and wind/jet velocity in the range $1000 - 3000 \text{ km s}^{-1}$.

If the kinetic energy of the jet is largely used to accelerate the mass M of the ambient medium into the thin envelope, then we can assume conservation of kinetic energy, i.e.

$$\frac{1}{2} \dot{M}_j v_j^2 t = \frac{1}{2} M v_r^2. \quad (1)$$

We assume that the envelope is expanding at a velocity of $v_r = 40 \text{ km s}^{-1}$ over the life-time t of the nebula. This yields the mass of the swept-up ambient medium in the form

$$\begin{aligned} M &= \dot{M}_j t v_j^2 v_r^{-2} \\ &= 0.6 M_\odot \frac{\dot{M}_j}{10^{-7} M_\odot \text{ yr}^{-1}} \frac{t}{10^4 \text{ yr}} \\ &\quad \cdot \left(\frac{v_j}{1000 \text{ km s}^{-1}} \right)^2 \left(\frac{v_r}{40 \text{ km s}^{-1}} \right)^{-2}. \end{aligned} \quad (2)$$

For simplicity we assume a conical outline of the nebula and a uniform ambient medium of number density n , which is then calculated from

$$\begin{aligned} n &= \frac{3}{\pi} \frac{M}{m_p} l^{-1} r_0^{-2} \\ &= 80 \text{ cm}^{-3} \left(\frac{M}{0.6 M_\odot} \right) \left(\frac{l}{2 \text{ pc}} \right)^{-1} \left(\frac{r_0}{0.4 \text{ pc}} \right)^{-2}, \end{aligned} \quad (4)$$

where m_p is the mass of the hydrogen atom (we assume a pure hydrogen nebula). Since M is the mass of only one side of the envelope, complete envelope will have a mass of roughly $2M$. Via the size scale the density n is inversely proportional to the cube of the distance of KJPN 8. Using the distance of 1600 pc as determined by Meaburn (1997), the density of the ambient would be 330 cm^{-3} . Since the cooling time are inversely proportional to the density, an accurate determination of the distance to KJPN 8 is important for our model.

The number density n_j of the collimated jet can then be estimated from the ratio ζ between the jet velocity v_j and the bow-shock speed v_{jh} . From ram-pressure balance at the working surface of a supersonic jet, we have

$$n_j = n(\zeta - 1)^{-2}. \quad (5)$$

For a typical range of wind/jet velocities given above and the roughly estimated advance speed $v_{jh} = 400 \text{ km s}^{-1}$, ζ is in the range 2.5-7.5. This translates into a jet density between about 2 and 35 cm^{-3} for $n = 80 \text{ cm}^{-3}$.

The radius of the jet after collimation is then

$$\begin{aligned} r_j &= \left(\frac{1}{\pi m_p} \dot{M} n_j^{-1} v_j^{-1} \right)^{1/2} \\ &= 3.5 \times 10^{16} \text{ cm} \left(\frac{\dot{M}_j}{10^{-7} M_{\odot} \text{ yr}^{-1}} \right)^{1/2} \\ &\quad \left(\frac{n_j}{10 \text{ cm}^{-3}} \right)^{-1/2} \left(\frac{v_j}{1000 \text{ km s}^{-1}} \right)^{-1/2}. \end{aligned} \quad (6)$$

Using the range of mass loss, jet velocity and densities estimated above, the radius of the jet after collimation is within approximately one order of magnitude of $3.5 \times 10^{16} \text{ cm}$. This radius is similar to that of the CO molecular ring found by Huggins et al. (1997) and Forveille et al. (1998). The axis of the ring is aligned with the most recent high velocity jets. The possible relation of this toroid with a similar structure related to the origin of the bipolar large envelope is at present uncertain. However, it is interesting to note that this peculiar situation is not unique among PNe. Another example is found in the multipolar PN NGC 2440 (López et al. 1998) where HST images also reveal a toroidal structure at its core. The plane of this ring is not orthogonal to the axis of the main bipolar structure either. This is a problem in PN evolution that has not been addressed yet in any detail and clearly deserves further investigation. For this analysis we shall simply assume, without further consequences for the models, that a high density equatorial ring has been related to the collimation of the outflow, in a process similar to the one described by Mellema & Frank (1997).

For the formation of an extended envelope from a low-density jet a Mach number $M > 5$ is required (Norman, Smarr and Winkler 1985). A Mach number $M = 10$ yields a temperature of the jet given by

$$\begin{aligned} T_j &= \frac{\bar{m} v_j^2}{\gamma k M^2} \\ &= 3.6 \times 10^5 \text{ K} \left(\frac{M}{10} \right)^{-2} \left(\frac{v_j}{1000 \text{ km s}^{-1}} \right)^2. \end{aligned} \quad (7)$$

Here $\gamma = 5/3$ and \bar{m} is the mean molecular weight and k is the Boltzmann constant (we assume $\bar{m} = 0.5m_p$, m_p is the proton mass). For jet velocities of up to 3000 km s^{-1} and a Mach number fixed at $M = 10$, this yields a jet temperature of up to a few times 10^6 K .

A jet of this temperature and velocity is capable of producing a significant amount of thermal X-ray radiation. The highest intensity can be expected to emerge from the hot shocked jet gas in the stagnation region of the active jet. Diffuse emission should be found in the large volume of the still hot cocoon region. The emissivity ϵ_x from bremsstrahlung can be calculated from (Cox and Tucker, 1969)

$$\epsilon_x = 2.3 \times 10^{-27} \left(\frac{n}{1\text{cm}^{-3}} \right)^2 \left(\frac{T}{1\text{K}} \right)^{1/2}, \quad (8)$$

where T and n are the temperature and number density of the emitting gas, respectively. At a pre-shock velocity of 3000 km s^{-1} the post-shock temperature will be 10^8K . For an order of magnitude estimate of the expected X-ray emission in the stagnation region let's assume $n = 4n_j = 40 \text{ cm}^{-3}$ and an emitting volume $V = 4\pi r_j^3/3 = 4 \times 10^{51} \text{ cm}^{-3}$ ($r_j = 1 \times 10^{17} \text{ cm}$). This yields a total luminosity $L_x = 1.5 \times 10^{32} \text{ erg sec}^{-1}$. At a distance of 1 kpc this corresponds to an integrated flux of $1.3 \times 10^{-12} \text{ erg sec}^{-1} \text{ cm}^{-2}$ which would be within reach of the AXAF space telescope. Obviously, X-ray observations of KJPN 8 will be an important test of some aspects of our jet model.

2.1. Summary of estimated parameters

The estimated parameters for the envelope of KJPN 8 and the outflow, which has produced it, are:

$$\begin{aligned} t &\approx 10^4 \text{ yr} \\ n &\approx 80 \text{ cm}^{-3} \\ M &\approx 0.6 M_\odot \\ n_j &\approx 2 - 35 \text{ cm}^{-3} \\ r_j &\approx 3.5 \times 10^{15-17} \text{ cm} \\ v_j &\approx 1000 - 3000 \text{ km s}^{-1} \\ v_{jh} &\approx 400 \text{ km s}^{-1} \\ T_j &\sim 10^6 K \end{aligned}$$

The parameters are not all independent from each other. For instance, the advance speed v_{jh} of the bow-shock has been estimated from the expansion speed of the envelope and its

size (the latter in turn depends on the distance). Keeping the advance speed fixed, while changing the ambient density requires a corresponding change of the jet density or velocity. These changes of the jet parameters have strong implications for the cooling of the jet and thereby on the local radii of the jet and the envelope.

3. The free stagnation knot model

We now consider the required time-scales for the formation of the stagnation knot and estimate its basic properties like density and size. A schematic illustration of this mechanism is presented in Figure 2. The top diagram shows the out-flowing jet with the extended expanding envelope of shocked ambient gas. In the stagnation region a dense knot has formed from cooling shocked interstellar gas and propagates along with the bow-shock. After the outflow ceases (bottom) the pressure inside the envelope decreases and becomes more uniform. During this stage the stagnation knot continues to move along the axis and forms a narrow nose to the wide envelope.

For the formation of a dense knot in the stagnation region of the bow-shock, the cooling time of the shocked ambient medium in this region has to be smaller than the age of the outflow.

Taking the average advance speed v_{jh} of the jet head as the shock speed, the post-shock cooling time in the stagnation region is

$$t_{\text{cl}} = 2450 \text{ yr} \left(\frac{n}{80 \text{ cm}^{-3}} \right)^{-1} \left(\frac{v_{\text{jh}}}{400 \text{ km s}^{-1}} \right)^{3.26}. \quad (9)$$

Here we have used a cooling function of the form (e.g. Blondin, Fryxell and Königl)

$$\Lambda(T) = \Lambda_0 T^\alpha \quad (10)$$

with $\Lambda_0 = 1.05 \cdot 10^{-18} \text{ erg s}^{-1} \text{ cm}^{-3}$ and $\alpha = -0.63$ at $T > 1.5 \cdot 10^5 \text{ K}$. These values closely describe the cooling in the corresponding temperature regime in the numerical code used for our simulations. The temperature T immediately behind the shock is given by

$$T = \frac{3}{16} \frac{\bar{m}}{k} v_{\text{jh}}^2. \quad (11)$$

The outflow must have lasted and kept its direction for a period longer than this value. Otherwise the gas in the stagnation region might not cool before flowing off into the cocoon. The cooling time t_{cl} thereby represents a lower limit to the duty cycle of any intermittence of the outflow. The value is however rather uncertain, due to the strong dependence on the

advance speed of the bow-shock v_{jh} , which is not well known for KJpN 8. A higher ambient density n would make the process more efficient, reducing the cooling time proportionally. Even within the uncertainty of a factor of two for the bow-shock speed, the stagnation knot should be formed quite early within the estimated age of the nebula ($t < 10^4$ yr).

As long as the knot does not brake up and is highly supersonic (as is the case here) it is “free” to continue its motion through the ambient medium until it has swept up roughly as much mass as its own. The distance d which it will reach by then is

$$d = \frac{4n_{\text{k}0}}{3n}r_{\text{k}0}, \quad (12)$$

where $n_{\text{k}0}$ and $r_{\text{k}0}$ are the number density and the spherical radius of the knot, respectively. The density is estimated by assuming that the knot is in pressure equilibrium with the surrounding medium in the stagnation region, which has roughly the same thermal pressure as the ram pressure of the jet. For the final temperature of the knot it appears reasonable to assume roughly $T = 10^4$ K. The number density of the knot is then

$$\begin{aligned} n_{\text{k}0} &= n_{\text{j}} \frac{\bar{m}v_{\text{j}}^2}{kT} \\ &= 6 \times 10^4 \text{ cm}^{-3} \frac{n_{\text{j}}}{10\text{cm}^{-3}} \left(\frac{T}{10^4 \text{ K}} \right)^{-1} \left(\frac{v_{\text{j}}}{1000 \text{ km s}^{-1}} \right)^2 \end{aligned} \quad (13)$$

where \bar{m} is the mean atomic mass (assumed to be half a hydrogen atom to account for ionization) and k is the Boltzmann constant. Using the values estimated in Section 2 the density in the knot is $n_{\text{k}0} = 4.1 \times 10^5 \text{ cm}^{-3}$. We find an upper limit for its radius by assuming that only ambient gas can cool which is located within a jet radius r_{j} of the axis. Any gas further away from the axis will flow into the cocoon. For a knot that has been compressed to the density $n_{\text{k}0}$ it is then found that the spherical radius $r_{\text{k}0}$ is given by

$$\pi r_{\text{j}}^2 v_{\text{jh}} t n > \frac{4\pi}{3} r_{\text{k}0}^3 n_{\text{k}0}, \quad (14)$$

where v_{jh} is the advance speed of the bow-shock and t is the age of the source at the time when the cooling in the stagnation region becomes significant. Using Equation 5 in the approximation of a light jet ($\zeta \gg 1$) and combining it with Equations 13 and 14, the upper limit for the radius of the knot is

$$\begin{aligned} r_{\text{k}0} &< \left(\frac{3}{4} r_{\text{j}}^2 \frac{t}{v_{\text{jh}}} \frac{kT}{m} \right)^{\frac{1}{3}} \\ &= 4.6 \times 10^{16} \text{ cm} \cdot \\ &\quad \left[\left(\frac{r_{\text{j}}}{10^{17} \text{ cm}} \right)^2 \frac{t}{10^4 \text{ yr}} \frac{T}{10^4 \text{ K}} \left(\frac{v_{\text{jh}}}{400 \text{ km s}^{-1}} \right)^{-1} \right]^{\frac{1}{3}}. \end{aligned} \quad (15)$$

Applying the estimates for n_{k0} and r_{k0} to Equation 12 we find $d_s = 4.6 \times 10^{19}$ cm = 15 pc, which is interpreted as an upper limit to the distance the stagnation knot can travel. A lower limit for this distance can be estimated by considering the expansion of the knot. As long as the outflow is active, the stagnation knot will be confined by the pressure in the bow-shock region and advance at the bow-shock speed. Once the outflow ceases the pressure will fall, allowing the stagnation knot to increase its radius roughly with its internal sound speed c_s . The sound crossing time corresponding to $r_{k0} = 4.6 \times 10^{16}$ cm is $t_s = 3.8 \times 10^{10}$ s. If the knot moves at $v_{jh} = 400$ km s $^{-1}$, then it will travel a distance $d_s = 1.2 \times 10^{18}$ cm ≈ 0.4 pc in this time. Assuming that the knot can survive a few times the sound crossing time before it fully disintegrates and stops, then the knot can travel for a distance of the order of 1 parsec (for the typical parameters used in Equation 15). These values are consistent with the observed distance of 2 parsec between the central source and the tip of the envelope of KJPN 8.

4. Numerical simulations

The numerical simulations have been carried out with the adaptive grid hydrodynamic code described by Raga (1994) in axisymmetric and slab-symmetric mode. This code solves the equations of mass, momentum and energy conservation using a flux-vector-splitting scheme (van Leer 1982). The computations were carried out on a 5-level, binary adaptive grid. The maximum grid size was 1025×513 and 513×513 cells in the case of axial and plane symmetries, respectively. The non-equilibrium cooling as described in Biro, Raga and Cantó (1995) has been used. For low temperatures, energy loss from the collisional excitation of [O I] and [O II] lines and radiative recombination of H have been taken into account. At temperatures higher than 5×10^4 K, a parameterised coronal equilibrium cooling rate is used. The collisional ionization of H and excitation of Lyman-alpha are also included in the cooling. The boundary conditions were reflective on the axis and on the left side of the computational domain (except for the inflow condition where the jet is injected). For the top, bottom (in plane symmetry) and right boundaries outflow conditions were applied. The jet is injected with uniform velocity and density over its radius. The H α emissivity has been calculated using radiative recombination (Case B) and collisional excitation following Aller (1984).

The slab-symmetric simulation presented in the next section is used to illustrate the qualitative details of the formation of the stagnation knot while excluding possible singular numerical effects on the axis of the axisymmetric computation. Parameters of the slab-symmetric simulation have been chosen for clarity of illustration of the mechanism of the formation of the stagnation knot, rather than for comparison with KJPN8. For a more

detailed comparison with the observations of KJpN8, we use an axisymmetric model, since it provides a more realistic calculation of the off-axis kinematics and the emission of the envelope, as well as for the compression and kinematics of the free stagnation knot.

4.1. Results and discussion

A series of simulations was performed in which we investigated the effects of varying the densities of the jet and the ISM ($n_j = 0.1 - 20 \text{ cm}^{-3}$; $n_{\text{ISM}} = 1 - 150 \text{ cm}^{-3}$), the jet velocity ($v_j = 500 - 4000 \text{ km s}^{-1}$), its initial radius ($r_j = 0.5 - 3 \times 10^{17} \text{ cm}$), the jet half opening-angle ($0 - 25^\circ$) and the grid resolution (up to 1025×513 grid points at the lowest level of the adaptive grid). As a final step we studied the effect of jet pulsation on the set of parameters that appeared to fit best the characteristics of KJpN 8. To ensure sufficient resolution over the jet radius, radii smaller than $0.5 \times 10^{17} \text{ cm}$ were not investigated.

The tests on the grid showed that at the highest resolution only the quantitative details of the simulations were still somewhat dependent on the resolution, especially those relevant to the cooling of the jet and the stagnation knot. Also, the detailed structure of the instabilities in the cocoon envelope slightly changed with resolution at early times, while it was still confined by the over-pressured cocoon. Increasing the resolution above the 1025×513 used in the simulations shown in this paper would have led to prohibitively high computing times.

The intermittence of the jet on a time-scale of around 1000 yr adds to the quasi-conical shape of the nebula as opposed to a more cylindrical shape obtained for a continuous ejection of the same jet. However, it is not clear from the simulations what exactly determines how the intermittence changes the shape. Relevant quantities could be the on/off ratio or the ratio between the times of the duty-cycle and the quasi-periodic vortex shedding near the head of the jet. The intermittence also emphasizes the division of the envelope into a few sections of different radii separated by rings of higher emissivity. In Section 2 we used this to estimate the duty-cycle of the episodic jet.

In the following, we describe representative simulations with very different jet parameters which all show the formation of the stagnation knot. These include one slab-symmetric run for a detailed demonstration of the formation process. The other two simulations are performed using cylindrical symmetry, one with a fully collimated jet and the other with a large opening angle. The parameters of these runs are listed in Table 1.

Figure 3 shows several stages of the formation of the stagnation knot during the slab-symmetric run. The images are grey-scale representations of the density (Fig. 3, Panels a,b

and d) and pressure (Figure 3, Panel c) with velocity arrows superimposed. Panels b and c of Figure 3 are density and pressure representations for the same time during the simulation. Only the bow-shock section from the larger full domain of the calculation is shown. Note that the velocity vectors are shown in the reference frame moving along with the bow-shock at speed v_{jh} as calculated from ram-pressure balance (equivalent to Eq. 5), i.e.

$$v_{\text{jh}} = \frac{v_j}{1 + \sqrt{\frac{n}{n_j}}}. \quad (16)$$

This changes the velocity vectors in the stagnation region to zero length. The validity of this condition can be appreciated in Figure 3, Panel a, where the velocity vectors in the stagnation region effectively have zero-length. Transforming the velocities to this system makes it easier to note the changes imposed by the cooling of the stagnation region. For clarity, vectors corresponding to velocities higher than 300 km s^{-1} in this frame have been omitted. The longest velocity vectors in the immediate post-shock region of the bow-shock correspond to $0.25v_{\text{jh}}$ which is approximately 100 km s^{-1} . Initially, the post-shock region of the ISM is roughly uniform in density ($t=700 \text{ yr}$, Fig. 3, Panel a). All the velocity vectors point along or diverge from the axis of the jet. At $t=1200 \text{ yr}$ the regions of highest density begin to cool noticeably and after 60 more years a significant increase in density and a decrease in pressure is seen (Panels b and c, respectively).

The reduction in pressure in the stagnation region causes a dramatic change in the structure of the bow-shock, shaping it concave instead of convex near the axis (Fig. 3, Panel d). In the concave region the swept-up ISM is now refracted towards the stagnation region thereby feeding the newly formed cold knot with fresh material. As can be seen from the short vectors associated with the cold knot, its velocity is very well reproduced by Equation 16. Given the reduced pressure, material is being accelerated towards the cold dense plug. This is best seen in Figure 3, Panel d, where both shocked gas from the jet and the ISM converge towards the stagnation knot from both sides. This is indicated by the presence of velocities of the order 100 km s^{-1} in the frame of the stagnation region (as defined by Equation 16).

The process observed here is similar to the formation of a nose cone in the case of a jet which is denser than the ambient medium. In that case the condensing material is from the jet which is refracted towards the axis in a concave jet-shock (Raga, Cantó & Cabrit 1998). Note that shortly after cooling the stagnation knot already shows signs of instability and fragmentation, which is important for its future development after the jet ceases and the condensation is set free. As discussed before, the compactness and therefore the degree of fragmentation strongly determines the distance the free stagnation knot can travel.

The formation of a stagnation knot in the axisymmetric run can be observed in Figure

4. The condensation moves outwards at the bow-shock speed, remaining at the boundary of the large-scale nebula. In this simulation the dense knot started to grow after approximately 1250 yr. Despite of the very different jet parameters, the cooling time is similar to the one found in the slab-symmetric simulation, since the advance speed of the bow-shock is approximately the same in both cases. The stagnation knot remains confined until the jet is switched off (at $t = 3470$ yr, after a period of intermittence with a duty-cycle of $t = 1260$ yr). After this time the knot starts to expand as the pressure in the cocoon drops (Figure 5). The high momentum keeps the knot propagating freely into the ambient medium at the original speed of the bow-shock for some time. Consequently, it starts to speed ahead of the original wide bow-shock, ploughing a narrow channel or ‘nose’ into the ISM. At the same time it increases its radius and flattens into a pancake-shaped slab. Instabilities cause it to form ripples which develop into individual smaller knots, resulting in a break-up of the original stagnation knot. The advance speed of the knot clearly decreases and an extrapolation shows that it would stop after traveling a distance of at most 1.5 pc from the point at which the jet was switched off (≈ 2.5 pc from the source). This value is in good agreement with the estimates in Section 4 and with the position of the observed end of the nebula in KjPn 8.

Figure 6 shows the time evolution of the $H\alpha$ emission from the simulated nebula from $t = 2840 - 9150$ yr as seen from a viewing angle almost perpendicular to the axis. It shows how the stagnation knot is compact at the beginning and then becomes diffuse as the pressure is not maintained by the jet anymore. In the last image the shape of the whole nebula is very similar to the envelope around KjPn 8 (Figure 1). The stagnation knot appears as a flat tip of the narrow nose very much like the observed one. Especially the north eastern lobe of the nebula is very well reproduced by the simulation, with the bright tip at the end associated with the stagnation knot. The surface brightness of the inner bulge of the nebula is higher than in the sections where the axial radius drops markedly. This is also found in the simulation, together with a good reproduction of the ripples caused by instabilities and intermittence of the jet.

After the jet injection ceases the pressure in the cocoon slowly decreases and the expansion of the envelope near the base slows down rather quickly below 50 km s^{-1} . In Figure 7 the position-velocity (pv) diagrams of the $H\alpha$ emissivity are shown (top and right panels). They correspond to the final stage of the time-series in Figure 6. In these diagrams position runs along the white dotted line, which also marks the location of zero expansion velocity. Positions in the pv-diagrams project directly onto the $H\alpha$ image, also shown (lower left). The diagrams represent thin slices through the cylindrical simulation. The ‘slit’ in the top diagram runs along the axis, while the other runs perpendicular to the axis (but looking along it). Only one of the two symmetric sections in the cut through the cylindrical envelope have been shown (exactly as represented by the $H\alpha$ image).

The expansion velocities at a time around 6000 yrs - corresponding to the fifth panel from the top in Figure 6 - are consistent with those measured for KJPn 8. After that, they fall below the observed value of 40 km s^{-1} to approximately 25 km s^{-1} . In the top pv-diagram of Figure 7 the velocity pattern drastically changes at the position where the inner wide envelope ends and the nose caused by the stagnation knot starts. This kinematic signature could be used as a further test performing spectral observations aiming at mapping the velocity field in the the corresponding area of KJPn 8. The currently available observations do not cover this area suitably.

The formation of the stagnation knot may be favoured by the axi-symmetric nature of the simulations. In this symmetry no change in direction of the outflow is allowed by possible jet-instabilities or deflections due to pressure variations in the cocoon. Changes of the flow direction would allow the gas in the stagnation region to flow off into the cocoon. The formation of the stagnation knot is therefore most likely to occur before the first internal reflection shock of the jet forms if the cooling time in the stagnation region is sufficiently short. In fact, even if the bow-shock speed was small enough, in none of the simulations performed a stagnation formed if a reflection shock was present before the stagnation region had time to cool. Instead, the whole bow-shock region would cool, producing a thin shell rather than a substantial axial knot. We attribute this to the shape of the bow-shock, which does not become concave, even after the cooling starts. The reason for this may be that, after the reflection shock, the radial momentum distribution in the jet peaks on the axis. This prevents the formation of a concave working surface.

If the outflow has a substantial opening angle, it is less sensitive to instabilities which temporarily could change its flow direction. In Figure 8 we present a simulation with an outflow which is poorly collimated and does not recollimate. Here the working surface and the stagnation region are larger compared to more collimated jets, resulting in a longer time available for cooling. Bow-shock velocities of flows with high opening angles decrease with increasing size of the shocked region, resulting in smaller cooling times for the shocked ISM. This further favours the formation of a stagnation knot. However, the knot has to form in the early stages of expansion before the bow-shock becomes fully radiative, otherwise only a thin convex shell is formed. Thus, a large finite opening-angle has interesting effects as it can improve the conditions for the formation of a stagnation knot if the jet does not recollimate. This occurs from a half-angle of approximately 20° on (Falle 1991, Peter & Eichler 1995). In such a case the shape of the envelope adopts a rather “boxy” structure when viewed from an angle perpendicular to the cylindrical axis (see Figure 8). This structure is similar to those found in some proto-planetary nebulae on a smaller scale, which so far have lacked a natural explanation (Bryce et al. 1997). Although in the present paper this is not explored further, a similar model might apply to these “boxy” PNe.

The extraordinary nature of the planetary nebula KjPn 8 appears to be linked to its environment. The quantitative conclusions from our model depend on the density of the ISM right before the formation of the nebula. Density variation over the size-scale of the envelope may be responsible for some of the asymmetries found in the giant envelope. For instance, the absence of a bright tip at the end of the SE arm could be related to a strong decrease in density. Sensitive searches of PNe embedded in diffuse clouds in the galactic plane might turn out more similar cases of wind/environment interactions.

Although the main focus of this work has been on the dynamical modeling of the giant envelope of KjPn 8, it is nevertheless of interest to add a note on the possible nature of the progenitor of KjPn 8. The nebula is outstanding among PNe and as such an uncommon origin may be expected. One clue may lie in the ionic abundances of the nebular core derived by Vázquez, Kingsburgh & López (1998). These authors find that KjPn 8 is an extreme type I PN with remarkably high ratios of He/H and Ne/O and similar to those found in He 2-111, another giant bipolar PN with high expansion velocities (Meaburn & Walsh 1989). PNe of type I are produced by massive progenitors and are generally bipolars (Peimbert & Torres-Peimbert 1983; Corradi & Schwarz 1995). Furthermore, Yungelson, Tutukov & Livio (1993) have discussed the type of binary systems that may lead to He rich PN envelopes which also involve massive progenitors that produce CO or ONe white dwarf nuclei. Coalescence of the binary nucleus during the AGB stage and more than one common envelope event and envelope ejection are possible paths in their analysis.

PNe are formed from stars with ZAMS masses $0.8 \lesssim M/M_{\odot} \lesssim 10$, however, most PNe show remnant cores of $\sim 0.6 M_{\odot}$, corresponding to progenitors of around 2 - 3 M_{\odot} . PNe with high-mass progenitors form spectacular and complex envelopes such as NGC 2440 and NGC 6302; these are bipolar type I PNe with core masses estimated around 0.8 - 0.9 M_{\odot} and must have originated from progenitors of $\sim 6 - 7 M_{\odot}$ (e.g. Pottasch 1983).

Thus, with these considerations, a reasonable possibility, although at this stage necessarily speculative, is to consider that objects like KjPn 8 and He 2-111 may have their origin in extremely massive progenitors, those located in the high-mass tail of the distribution of objects that produce PNe. This type of objects can be expected to be rare for in addition to the intrinsic lower number of available progenitors, their evolution as PNe would be very fast across the H-R diagram.

One further point that is worth mentioning is the presence of the high-velocity jets in KjPn 8 oriented at a substantially different position angle from the main symmetry axis of the main bipolar envelope. This secondary and younger jet system could in principle be interpreted as the result of some sort of rotation of the symmetry axis, as has been done in the case of Fleming 1 (López, Meaburn & Palmer 1993) and numerically simulated by Cliffe

et al. (1995). However, as discussed in Section 2 of this paper, the recent discovery of an expanding molecular ring or toroid whose plane is perpendicular to the high-velocity jets and consequently far off-axis from the main bipolar envelope (Forveille et al. 1998), represents now a severe obstacle for that interpretation. The analogous case of NGC 2440 has also been mentioned. In these cases it becomes interesting to consider the possibility of a recurrent envelope ejection after either coalescence of a binary nucleus, additional common envelope event, thermal flash or fast evolution of a secondary component. The resultant symmetry axis of the bipolar outflow and presumably the associated dense toroidal shells may have a different orientation in this occasion due to the dynamical perturbations occurring in the core. Within this picture, the cases where secondary jet systems are related to toroidal structures - which in turn are tilted with respect to the original bipolar envelopes - may possibly be understood. Otherwise the confronting elements are difficult to reconcile within our present limited understanding of PN formation and evolution.

5. Conclusions

A hydrodynamical model for the formation and evolution of the peculiar, giant, bipolar envelope of the planetary nebula K_jPn 8 has been investigated in analytical and numerical form. In this model a dense knot is formed from the shocked interstellar medium in the stagnation region of a supersonic episodic jet if the cooling time is smaller than the dynamical time needed for the shocked ISM to flow off into the cocoon of the jet. During the quiescent phase the knot conserves enough momentum and continues propagating freely, producing a distinct nose and a bright tip at the end of the lobe. From the analytical and numerical calculations it is concluded that the free stagnation knot model successfully reproduces the peculiar shape and kinematics of the giant envelope of the extraordinary planetary nebula K_jPn 8.

6. Acknowledgements

We thank Alejandro Raga for permission to use and modify his hydrodynamic code CORAL and Jose Luis Gómez for providing the software for the volumetric rendering of the axisymmetric emissivity data of the simulations. WS acknowledges the receipt of a PPARC research associateship and travel support from UNAM-DGAPA grant IN11896 for a visit to the IAUNAM-Ensenada during which part of this research was done. JAL acknowledges financial support from UNAM-DGAPA projects IN11896 and 101495. The authors acknowledge fruitful discussions with J. Meaburn, M. Bryce and G. García-Segura. We thank the

referee, Adam Frank, of stimulating suggestions that improved the presentation of this work.

REFERENCES

- Aller L., 1984, *Physics of Thermal Gaseous Nebulae*. Reidel, Dordrecht, p76
- Biro S., Raga A.C., Cantó J., 1995, *MNRAS*, 275, 557
- Blondin J.M, Fryxell B.A., Königl A., 1990, *ApJ*, 360, 370
- Bryce M., Pedlar A., Muxlow T., Thomasson P., Mellema G., 1997, *MNRAS*, 284, 81
- Cliffe J.A., Frank A., Livio M., Jones T.W., 1995, *ApJ*, 447, L49
- Corradi R.L.M., Schwarz H.E., 1995, *A&A*, 293, 871
- Cox D.P., Tucker W.H. 1969, *ApJ*, 157, 1157
- Peter W., Eichler D., 1995, *ApJ*, 438, 244
- Falle S.A.E.G., 1991, *MNRAS*, 250, 581
- Forveille T., Huggins P.J., Bachiller R., Cox P., 1998, *ApJ*, 495, L111
- Huggins P.J., Forveille T., Bachiller R., Cox P., 1997, *AAS*, 191, 1504
- Hutsemékers D., Surdej J., 1989, *A&A*, 219, 237
- Icke V., 1988, *A&A*, 202, 177
- López J.A., Meaburn J., Palmer J.R., 1993, *ApJ*, 415, L135
- López J.A., Vázquez R., Rodríguez L.F., 1995, *ApJ*, 455, L63
- López J.A., Meaburn J., Bryce M., Rodríguez L.F., 1997, *ApJ*, 475, 705
- López J.A., Meaburn J., Bryce M., Holloway A.J., 1998, *ApJ*, 493, 803
- Meaburn J., Walsh J.R., 1989, *A&A*, 223, 277
- Meaburn J., 1997, *MNRAS*, 292, 11
- Mellema G., Frank A., 1997, *MNRAS*, 292, 795

- Norman M.L., Smarr L., Winkler K.-H. A., 1985, in *Numerical Astrophysics*, Centrella J., LeBlanc J., Bowers R., Wilson J.R., eds, Jones and Bartlett Publisher, p88
- Peimbert M., Torres-Peimbert S., 1983, in IAU Symp. 103, Planetary Nebulae, ed. R.D. Flower (Dordrecht;Reidel), p 233
- Pottasch S.R., 1983, Planetary Nebulae, ASSL vol. 107, Reidel
- Raga, A.C., 1994, in *Stellar and Circumstellar Astrophysics*, eds. G. Wallenstein and A. Noriega-Crespo, PASP Conf. Proc., 57, 85
- Raga A.C., Cantó J., Cabrit S., 1998, A&A, 332, 714
- Steffen W., Gómez J.L., Williams R.J.R., Raga A.C., Pedlar A., 1997, MNRAS, 286, 1032
- van Leer, B., 1982, *Lecture Notes in Physics*, 170, 507
- Vázquez R., Kingsburgh R.L., López J.A., 1998, MNRAS, 296, 564
- Yungelson L.R., Tutukov A.V., Livio M., 1993, ApJ, 418, L135

		COLLIMATED	UNCOLLIMATED	SLAB
1/2 opening angle	θ	0	25	5
jet radius	r_j	0.1	0.15	0.075
jet velocity	v_j	3000	4000	1100
jet density	n_j	3	1.25	30
jet temperature	T_j	2×10^6	2×10^6	2×10^5
mass loss rate	\dot{M}_j	7.4×10^{-7}	7.4×10^{-7}	7.7×10^{-7}
ISM density	n	100	25	80
ISM temperature	T	10^4	10^4	10^4
domain of simul.		12×1.5	10×5	3×1.5
on/off times		0.3/0.1	—	—
cut-off time		1.2	3.2	—

Table 1: The parameters of the representative runs showing the stagnation knot with a fully collimated jet, an outflow with a large opening-angle of 25° and a slab-symmetric run with a small opening-angle. Lengths are given in units of 10^{18} cm and times are in units of 10^{11} sec. Number densities are given in units of 1 cm^{-3} , velocities in km s^{-1} and temperatures in Kelvin. The mass loss rate is given in solar masses per year.

Fig. 1.— Top: An $H\alpha$ mosaic of the giant ($14' \times 4'$) bipolar envelope of the planetary nebula KJPN 8 (López et al. 1995). Bottom: Enlargement of the NE region.

Fig. 2.— Schematic view of the stagnation knot scenario before (top) and after the outflow stops.

Fig. 3.— A slab symmetric simulation of the formation of the stagnation knot. Only the section of the bow-shock of a larger area of simulation is shown, which comprises the complete region affected by the interaction of the jet with the interstellar medium.

Fig. 4.— Evolution of the logarithmic density distribution of the axi-symmetric run starting at time $t = 1260$ yr and ending at $t = 8830$ yr. The pairs of logarithmic minimum and maximum for the individual images are (from top to bottom): $(-0.9, 4.6)$, $(-1.5, 4.6)$, $(-1.7, 6.1)$, $(-1.7, 4.1)$, $(-1.9, 4.2)$, $(-1.9, 3.9)$.

Fig. 5.— Logarithmic pressure distribution corresponding to the density distribution shown in Figure 4. The pairs of logarithmic minimum and maximum for the individual images are (from top to bottom): $(-10.1, -7.0)$, $(-11.0, -6.9)$, $(-11.7, -5.7)$, $(-11.5, -7.5)$, $(-11.0, -7.4)$, $(-11.4, -7.7)$.

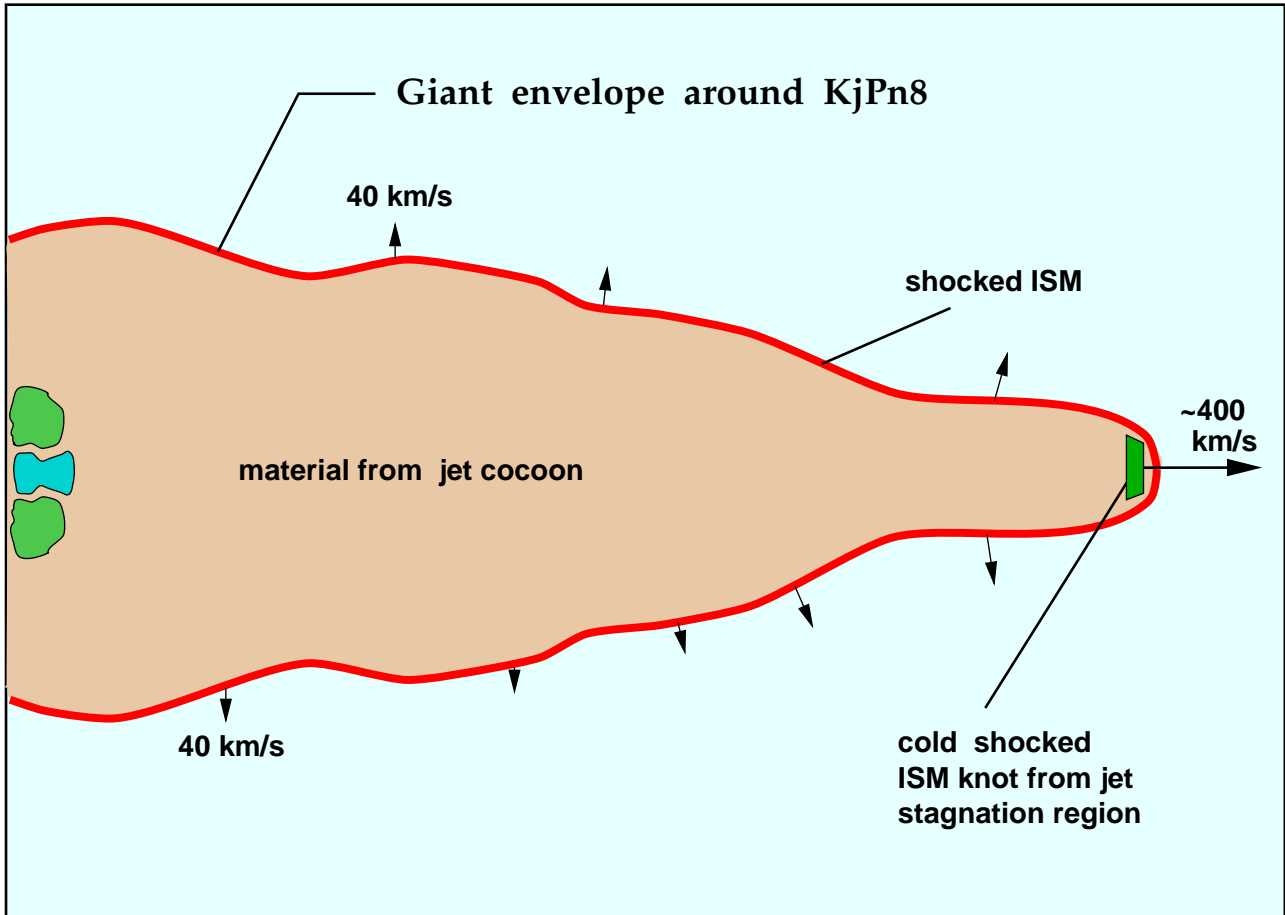
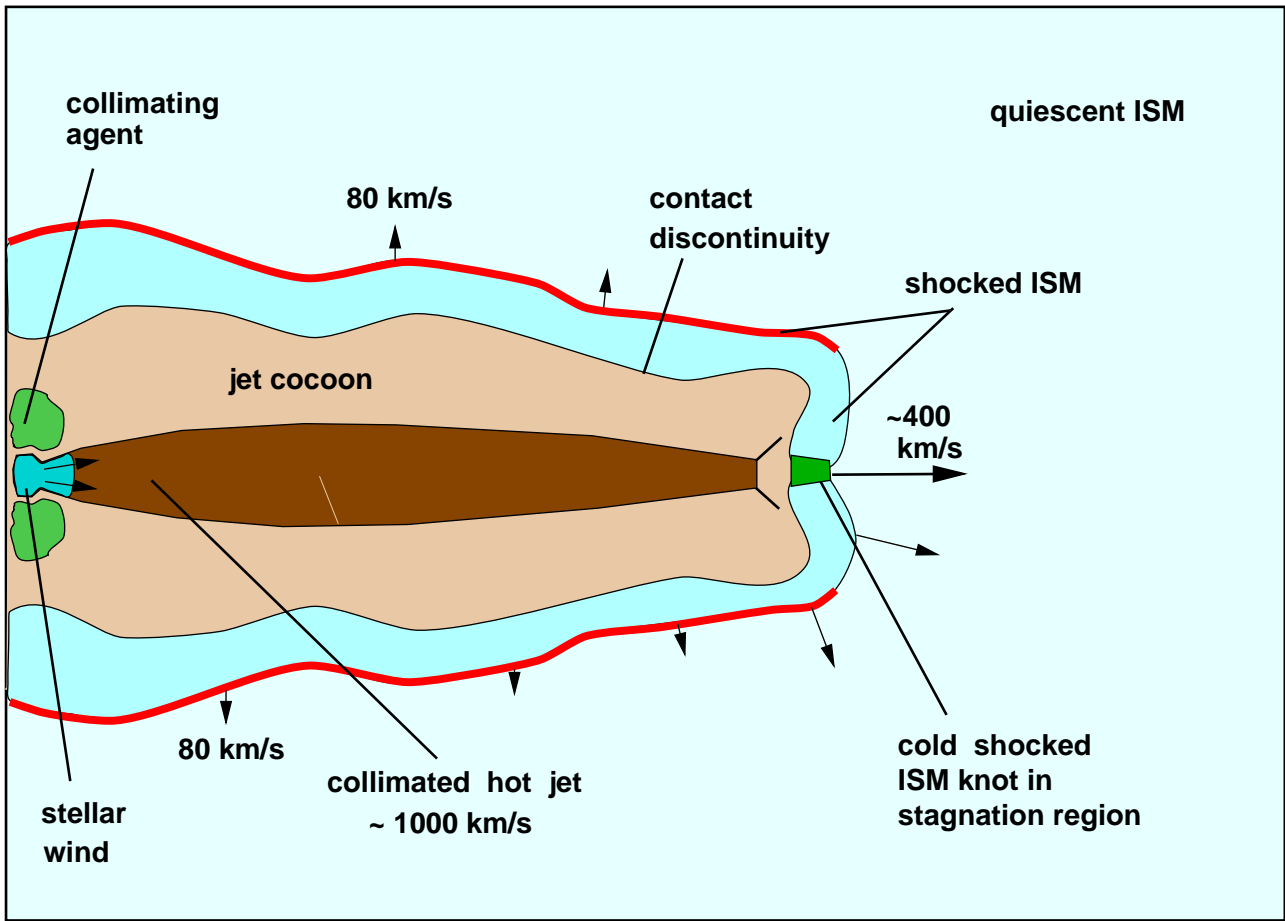
Fig. 6.— Volumetric rendering of the $H\alpha$ -emission from the simulation of the stagnation knot scenario (log-scale). The interval between the individual frames is 1578 years, beginning at 2840 years after the start of the simulation. Note the deceleration of the stagnation knot, soon after it expands and breaks up.

Fig. 7.— Position-velocity diagram of the envelope for a slit running along the axis of the envelope (top) and perpendicular to it, looking down the axis (right). The dotted lines mark zero expansion velocity. The emission of the stationary external medium has been suppressed in the pv-diagrams. The bottom left picture shows the logarithmic $H\alpha$ emissivity distribution as a positional reference to the pv-diagrams. In the pv-diagrams position runs along the white dotted line. The axial length-scale has been stretched by a factor of two as compared to the axial scale (see scale indicators in image).

Fig. 8.— The logarithmic density distribution of the nebula and stagnation knot formed from an outflow with an initial half-opening angle of 25° .

This figure "Fig1.jpg" is available in "jpg" format from:

<http://arxiv.org/ps/astro-ph/9807021v1>



This figure "Fig3.jpg" is available in "jpg" format from:

<http://arxiv.org/ps/astro-ph/9807021v1>

This figure "Fig4.jpg" is available in "jpg" format from:

<http://arxiv.org/ps/astro-ph/9807021v1>

This figure "Fig5.jpg" is available in "jpg" format from:

<http://arxiv.org/ps/astro-ph/9807021v1>

This figure "Fig6.jpg" is available in "jpg" format from:

<http://arxiv.org/ps/astro-ph/9807021v1>

This figure "Fig7.jpg" is available in "jpg" format from:

<http://arxiv.org/ps/astro-ph/9807021v1>

This figure "Fig8.jpg" is available in "jpg" format from:

<http://arxiv.org/ps/astro-ph/9807021v1>